JULY 31 2002

The propagation of sound in narrow street canyons

K. K. lu; K. M. Li

J. Acoust. Soc. Am. 112, 537–550 (2002)
https://doi.org/10.1121/1.1492821

The propagation of sound in narrow street canyons

K. K. Iu and K. M. Li[a)]
Department of Mechanical Engineering, The Hong Kong Polytechnic University, Hung Hom, Hong Kong

(Received 22 October 2001; revised 29 April 2002; accepted 20 May 2002)

This paper addresses an important problem of predicting sound propagation in narrow street canyons with width less than 10 m, which are commonly found in a built-up urban district. Major noise sources are, for example, air conditioners installed on building facades and powered mechanical equipment for repair and construction work. Interference effects due to multiple reflections from building facades and ground surfaces are important contributions in these complex environments. Although the studies of sound transmission in urban areas can be traced back to as early as the 1960s, the resulting mathematical and numerical models are still unable to predict sound fields accurately in city streets. This is understandable because sound propagation in city streets involves many intriguing phenomena such as reflections and scattering at the building facades, diffusion effects due to recessions and protrusions of building surfaces, geometric spreading, and atmospheric absorption. This paper describes the development of a numerical model for the prediction of sound fields in city streets. To simplify the problem, a typical city street is represented by two parallel reflecting walls and a flat impedance ground. The numerical model is based on a simple ray theory that takes account of multiple reflections from the building facades. The sound fields due to the point source and its images are summed coherently such that mutual interference effects between contributing rays can be included in the analysis. Indoor experiments are conducted in an anechoic chamber. Experimental data are compared with theoretical predictions to establish the validity and usefulness of this simple model. Outdoor experimental measurements have also been conducted to further validate the model.
[DOI: 10.1121/1.1492821]

PACS numbers: 43.50.Gf, 43.28.En, 43.50.Rq [MRS]

I. INTRODUCTION

The investigation of sound propagation outdoors has been the subject of extensive research since the 1950s. Piercy *et al.*[1] reviewed the development prior to 1977. Embleton[2] has summarized many intriguing features of outdoor sound by emphasizing field measurements and their physical interpretations. Most of these studies consider a relatively simple scenario—the source and receiver are located in the vicinity of an absorbing ground surface. However, due to the rapid urbanization of many countries and heightened environmental and other concerns in the past three decades, knowledge of the near-ground propagation of sound in complex urban environments is of great economic and social importance.

Indeed, theoretical studies of sound propagation in a city street were conducted in the 1970s by Schlatter,[3] Lee and Davies,[4] Lyon,[5] and Steenackers *et al.*[6] It was assumed in their analyses that the street was represented by a simple channel between two infinite-reflecting walls with image sources produced as a result of multiple reflections of sound. In their approach, attention was focused on the determination of a reverberant sound field in city streets. However, the possibilities of ground interference and further interference due to multiple reflections between two parallel walls were ignored in these early studies.

Oldham and Radwan[7] have proposed an alternative approach in which the sound levels in city streets are estimated by summing the sound intensities of direct and reflected sound. Kang[8] has compared the sound fields in street canyons with diffusely and geometrically reflecting boundaries. He has developed a radiosity-based theoretical model for diffusely reflecting boundaries. In his model, the sound propagation in the street can be simulated by energy exchange between the nodal points. The interference effects due to multiple reflections are expected to be less significant in the model. However, the radiosity approach is not included in the scope of our current study, but, rather, we prefer to study the interference effect of multiple reflections.

For geometrically reflecting boundaries, the energy response at the receiver is obtained by summing contributions from the source and all image sources. Some commercial software, such as Raynoise,[9] has implemented this idea to include the effect of wall/ground absorption in these models. However, the interference effects between the direct and reflected waves are again not included in their calculations. In addition, they have restricted their studies to the case where the width of the street canyon ranges from 10 to 40 m only. In some practical situations of a dense high-rise city, the width of many street alleys is often less than 10 m. This gives us a motivation to investigate the propagation of sound in this type of environment, which is referred as narrow street canyons in this paper.

We also note that Walerian *et al.*[10] have recently exploited a simple model for predicting the time-average sound level within an urban system. In their propagation model, a sound wave interacting with obstacles undergoes multiple

[a)]Author to whom correspondence should be addressed. Electronic mail: mmkmli@polyu.edu.hk

reflections from walls and diffractions from wedges. In the case of canyon streets, diffraction at the top edges of buildings has been omitted in their studies. Further, it is assumed that the total field is computed by summing the squared pressures of all image sources. As a result of using squared pressures in the summation, the interference effects are omitted in their analysis. Although Walerian *et al.* have pointed out that the interference effect is significant for a relatively narrow street canyon, no further investigations have been conducted.

In the late 1970s, Gensane and Santon[11] considered the wave nature of sound in their study for sound fields in bounded and arbitrarily shaped air spaces. Lemire and Nicolas[12] extended this approach by using a spherical wave reflection coefficient instead of a plane wave reflection coefficient to model sound wave propagation in a bounded space. In particular, they investigated the sound fields in a rectangular enclosure and the region bounded by two infinite parallel planes. Their predicted results agreed very well with the standard normal mode solutions, but no experimental validations were presented in their study. We also remark that Dance *et al.*[13] have pointed out the importance of interference effects in an enclosed space. By assuming perfectly reflecting boundaries and using an image-source method, they developed an interference model for calculating the total sound fields in an industrial space. However, their model was found to be more accurate near the vertical walls, floor, and ceiling, but less so at receivers located further from these reflecting surfaces. In view of these earlier studies, we endeavor to extend these models by considering theoretically and experimentally the effect of finite impedance on the overall sound fields in an enclosed space.

In this paper, we wish to investigate the propagation of sound in a narrow street such that the height of the buildings is much greater than the width of the street. It is expected that the interference effects caused by direct and reflected rays will play a significant role in the prediction of sound fields in such a street canyon. A brief review of other models is discussed also, but our principal aim is to establish a simple yet accurate model for predicting sound fields in narrow street canyons. The model is based on an analytic Green's function. We also conduct extensive experimental measurements both indoors and outdoors. Indoor experiments are conducted in an anechoic chamber and outdoor field measurements are carried out in a typical alley street. The theoretical predictions will be compared with the experimental measurements. The emphasis of this paper is the experimental verification of the proposed theoretical model.

II. PROPAGATION MODELS

A. Analytical formulations

In an earlier publication, Tang and Li[14] derived an expression for the sound field due to a harmonic source above an impedance ground in front of an absorbing facade. In this paper, we extend their work to consider the sound fields above an impedance ground between two parallel facade surfaces. This is the model we adopt to assess the sound propagation in a narrow city street. Essentially, the street is represented as two infinite vertical planes of normalized admittance, β_L and β_R, respectively. They are parallel, and located at the plane of $x=0$ for the left vertical wall and at the plane $x=W$ for the right vertical wall. An impedance ground of normalized admittance β_B, which is located between the vertical walls, is situated at the plane $z=0$. The impedance ground is assumed to be perpendicular to the vertical walls. The schematic diagram of the posed problem is shown in Fig. 1. We assume that a point source is placed at $(x_s,0,z_s)$, where the time-dependent factor, $e^{-i\omega t}$, is understood and suppressed throughout the analysis. As the sound field is symmetrical about the $y=0$ plane, we restrict our interest to the region where $x\in[0,W]$, $y\in[0,\infty)$, and $z\in[0,\infty)$. The sound field, $p(x,y,z)$, can be computed by solving the Helmholtz equation:

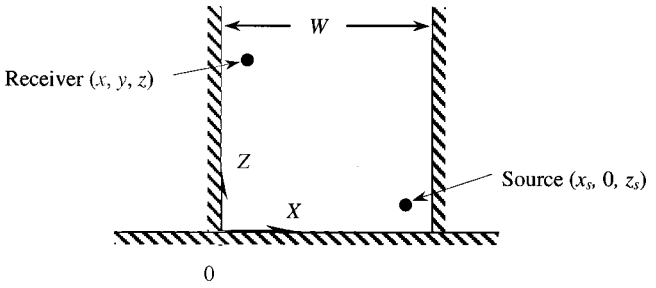

FIG. 1. Schematic diagram for sound propagation in a city street.

$$\nabla^2 p + k^2 p = -\delta(x-x_s)\,\delta(y)\,\delta(z-z_s), \tag{1}$$

where k is the wave number of the source. The governing equation is supplemented further by the boundary conditions of the parallel walls and the impedance ground as follows:

$$\frac{\partial p}{\partial x} + ik\beta_L p = 0 \quad \text{at } x=0, \tag{2a}$$

$$\frac{\partial p}{\partial x} - ik\beta_R p = 0 \quad \text{at } x=W, \tag{2b}$$

and

$$\frac{\partial p}{\partial z} + ik\beta_B p = 0 \quad \text{at } z=0. \tag{2c}$$

In the absence of the impedance ground, the solution can be expressed as a Fourier integral[15]

$$p = -\frac{1}{(2\pi)^3}\int_{-\infty}^{\infty}\int_{-\infty}^{\infty}\int_{-\infty}^{\infty}\frac{G_x \exp(ik_y y + ik_z|z-z_s|)}{(k^2-k_x^2-k_y^2-k_z^2)} \times dk_x\,dk_y\,dk_z, \tag{3}$$

taken over the space of all wavenumbers, $\mathbf{k}\equiv(k_x,k_y,k_z)$. The variable G_x in Eq. (3) may be regarded as the required Green's function in the wave number space given by

$$G_x=\begin{cases}\dfrac{[e^{-ik_x x_s}+V_L e^{ik_x x_s}][e^{ik_x x}+V_R e^{[ik_x(2W-x)]}]}{1-V_L V_R\exp(2ik_x W)} \\ \quad \text{for } x\geqslant x_s, \\ \dfrac{[e^{ik_x x_s}+V_L e^{ik_x x_s}][e^{-ik_x x}+V_R e^{[ik_x(2W-x)]}]}{1-V_L V_R\exp(2ik_x W)} \\ \quad \text{for } x<x_s, \end{cases} \tag{4}$$

where V_L and V_R are the reflection factors for the waves reflected by the left and right vertical walls, respectively. They can be determined according to

$$V_L=\frac{k_x-k\beta_L}{k_x+k\beta_L} \tag{5a}$$

and

$$V_R=\frac{k_x-k\beta_R}{k_x+k\beta_R}. \tag{5b}$$

Replacing the denominator by its binomial series, expanding the square brackets, and grouping all terms accordingly in Eq. (4), we obtain

$$G_x=\sum_{l=0}^{\infty}[e^{ik_x|x-x_s|}+V_L e^{ik_x(x+x_s)}+V_R e^{ik_x(2W-x-x_s)} + V_L V_R e^{ik_x(2W-x+x_s)}](V_L V_R e^{2ik_x W})^l. \tag{6}$$

First, let us consider the case when $l=0$ of the series in Eq. (6). The first term in the square bracket represents the direct wave. The second term in the square bracket is a result of the reflection from the left vertical wall. They are marked as S_{01} and S_{02} in Fig. 2. The last two terms are a pair of image sources, which are obtained by mirror reflection of the first two in the right vertical wall. They are marked as S_{03} and S_{04} in Fig. 2. The process can be repeated again and again (in which l ranges from 1 to ∞ in the series), leading to a row of an infinite number of image sources located at the height of z_s above the impedance ground. In the event that the waves are reflected by the impedance ground, we can apply the boundary condition (2c) in Eq. (3) to yield

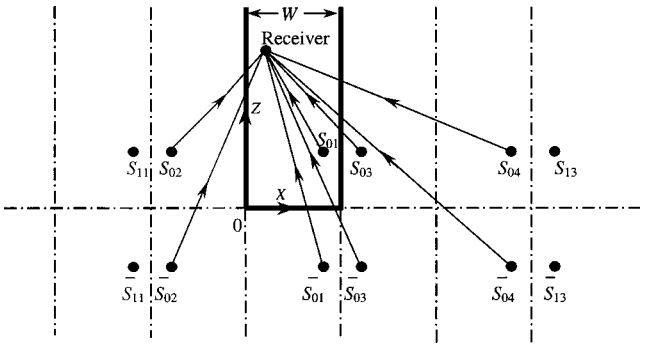

FIG. 2. Two rows of image sources are obtained by mirror reflection of the vertical walls and a reflecting ground. The source, S_{01}, is located at $(x_s,0,z_s)$ and the receiver at (x,y,z).

$$p=-\frac{1}{(2\pi)^3}\int_{-\infty}^{\infty}\int_{-\infty}^{\infty}\int_{-\infty}^{\infty}\frac{G_x e^{ik_y y}}{(k^2-k_x^2-k_y^2-k_z^2)} \times\{e^{ik_z|z-z_s|}+V_B e^{ik_z(z+z_s)}\}dk_x dk_y dk_z, \tag{7}$$

where V_B is the reflection factor of the waves from the ground, which can be expressed as

$$V_B=\frac{k_z-k\beta_B}{k_z+k\beta_B}. \tag{8}$$

The outer integral with respect to k_z can be evaluated by the method of contour integration[15] to give

$$p=\frac{i}{(2\pi)^2}\int_{-\infty}^{\infty}\int_{-\infty}^{\infty}\frac{G_x e^{ik_y y}}{2k_z^*} \times\{e^{ik_z^*|z-z_s|}+V_B^* e^{ik_z^*(z+z_s)}\}dk_x dk_y, \tag{9a}$$

where

$$k_z^*=+\sqrt{k^2-k_x^2-k_y^2} \tag{9b}$$

and

$$V_B^*=\frac{k_z^*-k\beta_B}{k_z^*+k\beta_B}. \tag{9c}$$

In this paper, the integral (9a) is used for the modeling of sound propagation in a street canyon. However, the exact evaluation of the integral is difficult if not impossible for all but the simplest situation. A well-known example is that all reflecting surfaces are acoustically hard where $\beta_B=\beta_L=\beta_R=0$. In this case, the reflection factors are all equal to 1, i.e., $V_L=V_R=V_B^*=1$. Substitution of Eq. (6) into (9a) leads to

$$p=\frac{i}{(2\pi)^2}\sum_{l=0}^{\infty}\int_{-\infty}^{\infty}\int_{-\infty}^{\infty}\frac{e^{ik_y y}e^{ik_z^*|z-z_s|}}{2k_z^*}[e^{ik_x|x-x_s|}+e^{ik_x(x+x_s)}+e^{ik_x(2W-x-x_s)}+e^{ik_x(2W-x+x_s)}](e^{2ik_x W})^l dk_x dk_y + \frac{i}{(2\pi)^2}\sum_{l=0}^{\infty}\int_{-\infty}^{\infty}\int_{-\infty}^{\infty}\frac{e^{ik_y y}e^{ik_z^*(z+z_s)}}{2k_z^*}[e^{ik_x|x-x_s|}+e^{ik_x(x+x_s)}+e^{ik_x(2W-x-x_s)}+e^{ik_x(2W-x+x_s)}](e^{2ik_x W})^l dk_x dk_y. \tag{10}$$

Obviously, the total sound field is composed of contributions from two rows of noise sources located at heights z_s and $-z_s$, respectively. Each of these integrals in Eq. (10) can be identified as a Sommerfeld integral with each source located at a different position. These integrals can be evaluated exactly (see, for example, Ref. 16), and the total sound field can be expressed as the sum of a series as follows:

$$p=\frac{1}{4\pi}\sum_{l=0}^{\infty}\left[\frac{e^{ikd_{l1}}}{d_{l1}}+\frac{e^{ikd_{l2}}}{d_{l2}}+\frac{e^{ikd_{l3}}}{d_{l3}}+\frac{e^{ikd_{l4}}}{d_{l4}}+\frac{e^{ik\bar{d}_{l1}}}{\bar{d}_{l1}}+\frac{e^{ik\bar{d}_{l2}}}{\bar{d}_{l2}}+\frac{e^{ik\bar{d}_{l3}}}{\bar{d}_{l3}}+\frac{e^{ik\bar{d}_{l4}}}{\bar{d}_{l4}}\right], \tag{11}$$

where the first four terms of the square bracket in the above series are the contributions due to the reflections from the vertical walls only. The path lengths, d_{l1}, d_{l2}, d_{l3}, and d_{l4} can be determined by simple geometrical considerations. The total sound field is also augmented by a set of image sources due to the presence of a reflecting ground. These are represented by the last four terms of the square bracket in Eq. (11). The corresponding path lengths are $\bar{d}_{l1}$, $\bar{d}_{l2}$, $\bar{d}_{l3}$, and $\bar{d}_{l4}$ that can also be determined straightforwardly.

The above theoretical formulation provides the basis for subsequent analyses. Two popular heuristic approximations, the incoherent and coherent models, will be described in the following sections.

B. A critical review of the incoherent model

Oldham and Radwan[7] have proposed a simple model for the prediction of sound propagated in a street canyon. The model is based on the construction of all image sources due to the reflections from the building facade on each side of the street. The total sound level is computed by summing the intensities of direct and all reflected sound levels incoherently. According to this model, the intensity of the sound field ($I\propto\overline{p^2}$) can be obtained from Eq. (11) by summing each contributing component incoherently to yield

$$I=I_{\mathrm{ref}}\,d_{\mathrm{ref}}^{\,2}\sum_{l=0}^{\infty}\left(\frac{1}{d_{l1}^2}+\frac{1}{d_{l2}^2}+\frac{1}{d_{l3}^2}+\frac{1}{d_{l4}^2}+\frac{1}{d_{l1}^2}+\frac{1}{d_{l2}^2}+\frac{1}{d_{l3}^2}+\frac{1}{d_{l4}^2}\right), \tag{12}$$

where I_{ref} is the reference sound intensity at a reference distance of d_{ref} from the source. An implicit assumption of this approach is that the mutual interference effects of the direct and all reflected waves are ignored. The assumption is justifiable because the existence of many possible rays is expected to smooth out the effect of interference. Benjegard[17] supported this assumption by arguing that typical distances between the source and the receiver in urban areas are shorter than in the case of major highways. As a result, the influence of any possible interference due to ground and facade reflections is insignificant for the propagation of sound. Chew[18] derived a model to predict sound fields for the case in which buildings flank both sides of an expressway. In his model, he followed the concept proposed by Davies,[19] which includes the effects of multiple reflections and diffuse scattering for noise propagated in street canyons. Reflection coefficients are used in their numerical method, leading to a better model for estimating the effects of ground and facade on the overall noise levels, but the direct wave and reflected waves are combined incoherently. In this paper, we refer to this type of prediction method as the incoherent model.

To allow for finite impedances of the facades and the ground surfaces, the concept of the absorption coefficient is sometimes introduced, such that a fraction of constant sound energy, α say, is absorbed for each reflection from the facades and impedance ground. In other words, the factor $(1-\alpha)$ is multiplied for each reflection from the reflecting boundaries. Hence, the total sound field can be estimated heuristically by

$$I=I_{\mathrm{ref}}\,d_{\mathrm{ref}}^{\,2}\sum_{l=0}^{\infty}\left(\frac{(1-\alpha_L)^l(1-\alpha_R)^l}{d_{l1}^2}+\frac{(1-\alpha_L)^{l+1}(1-\alpha_R)^l}{d_{l2}^2}+\frac{(1-\alpha_L)^l(1-\alpha_R)^{l+1}}{d_{l3}^2}+\frac{(1-\alpha_L)^{l+1}(1-\alpha_R)^{l+1}}{d_{l4}^2}+\frac{(1-\alpha_L)^l(1-\alpha_R)^l(1-\alpha_G)^{l+1}}{\bar{d}_{l1}^2}+\frac{(1-\alpha_L)^{l+1}(1-\alpha_R)^l(1-\alpha_G)^{l+1}}{\bar{d}_{l2}^2}+\frac{(1-\alpha_L)^l(1-\alpha_R)^{l+1}(1-\alpha_G)^{l+1}}{\bar{d}_{l3}^2}+\frac{(1-\alpha_L)^{l+1}(1-\alpha_R)^{l+1}(1-\alpha_G)^{l+1}}{\bar{d}_{l4}^2}\right), \tag{13}$$

where the subscripts L, R, and G represent the corresponding absorption coefficients for the left and right vertical walls and the impedance ground, respectively.

Building facades consist typically of brickwork or other masonry construction and glass windows. The absorption coefficient of brickwork varies from 0.02 at 125 Hz to 0.05 at 2 kHz. Windows, which act as panel absorbers, enhance the absorption at low frequencies. Delany[20] estimated the average absorption coefficient to be of the order of 0.1, taking into account the greater area of brickwork generally found in

traditional residential areas. In addition, Lee and Davies[4] studied the ground effect assuming the asphalt road surface to reflect 0.9 of the incident sound with no change in phase. Hence, it is reasonable for us to assume that all reflecting boundaries (including the vertical walls and the impedance ground) have the same absorption coefficients, i.e., $\alpha_L=\alpha_R=\alpha_G$. Indeed, Steenackers, Myncke, and Cops[6] determined the absorption coefficient of a typical urban street by measuring the decay curves of the reverberated sound in different streets and comparing them with calculated curves for different absorption coefficients. The absorption coefficient is determined by fitting the measured data with theoretical predictions. For streets of width ranging from 9 to 12 m, they found that the corresponding absorption coefficients vary between 0.1 and 0.2. In this paper, the absorption coefficient of 0.1 is used in our subsequent numerical analyses unless otherwise stated.

We also note that the direct sound pressure level is given, according to the incoherent model, by

$$L_D=L_{\text{ref}}+20\lg(d_{\text{ref}}/d_R), \tag{14}$$

where L_{ref} is the sound pressure level from the source at the reference distance and d_R is the distance between the source and receiver. The sound pressure level at the receiver due to a reflected ray ''hitting'' the boundaries n times is given by

$$L_{Rn}=L_{\text{ref}}+20\lg(d_{\text{ref}}/d_{Rn})+10n\lg(1-\alpha), \tag{15}$$

where n is the order of reflection, α is the absorption coefficient of the boundaries and d_{Rn} is the path length from the image sources to the receiver.

C. The coherent model

The incoherent model estimates the sound field by the energy approach in which the interference effects due to the source and its images are ignored. However, it becomes increasingly inadequate in some cases. A more accurate and intricate model is to allow the variation of the reflection factors, V_L, V_R, and V_B^*, with the angle of incidence in Eq. (9a). Before we proceed to give an analytical expression for the integrals in Eq. (9a), it is of interest to consider a special case where we have only an infinite facade, located at the left side, say, of the source. The theoretical and experimental studies of this case has been reported elsewhere.[14] In fact, this problem can be treated as a special case of two parallel walls where the width of the street becomes very large, $W\rightarrow\infty$. It is then straightforward to show $e^{ik_xW}\rightarrow 0$. We can simplify G_x from Eq. (4) to

$$G_x=e^{ik_x|x-x_s|}+V_Le^{ik_x(x+x_s)}. \tag{16}$$

Substituting it into Eq. (9a) leads to an analogous expression as developed in our earlier study[14] of sound fields above an impedance ground in front of an absorbing facade. An asymptotic solution has been derived in their study and it is given as follows:

$$\begin{aligned}p=&\frac{e^{ikd_{01}}}{4\pi d_{01}}+Q(d_{02},\theta_{02},\beta_L)\frac{e^{ikd_{02}}}{4\pi d_{02}}\\&+Q(\bar{d}_{01},\bar{\theta}_{01},\beta_G)\frac{e^{ik\bar{d}_{01}}}{4\pi d_{01}}\\&+Q(\bar{d}_{02},\bar{\theta}_{02},\beta_G)Q(\bar{d}_{02},\bar{\Theta}_{02},\beta_L)\frac{e^{ik\bar{d}_{02}}}{4\pi d_{02}},\end{aligned} \tag{17}$$

where $Q(d,\theta,\beta)$ is the spherical wave reflection coefficient[21] that can be determined for a given separation of the image source and receiver d, the angle of incidence of the reflected wave θ, and the normalized admittance of the boundary β. It is determined according to

$$Q(d,\theta,\beta)=R_p+(1-R_p)F(w), \tag{18}$$

where

$$R_p=\frac{\cos\theta-\beta}{\cos\theta+\beta}, \tag{19}$$

$$F(w)=1+i\sqrt{\pi}we^{-w^2}\operatorname{erfc}(-iw), \tag{20}$$

and

$$w=+\sqrt{\tfrac{1}{2}ikd}(\cos\theta+\beta). \tag{21}$$

The angle of incidence of the reflected waves, θ_{02}, $\bar{\theta}_{01}$, $\bar{\theta}_{02}$, and $\bar{\Theta}_{02}$ can be found for a given source and receiver location as

$$\begin{aligned}&\cos\theta_{02}=\frac{x+x_s}{d_{02}},\quad \cos\bar{\theta}_{01}=\frac{z+z_s}{\bar{d}_{01}},\\&\cos\bar{\theta}_{02}=\frac{z+z_s}{\bar{d}_{02}},\quad \text{and}\quad \cos\bar{\Theta}_{02}=\frac{x+x_s}{\bar{d}_{02}}.\end{aligned} \tag{22}$$

It is enlightening to show that our current theoretical formulation may be regarded as a generalization of the previous study.[14] Based on the analytical result of their approach, we can write down the heuristic solution for Eq. (9a) straightforwardly as

$$p=\frac{1}{4\pi}\sum_{l=0}^{\infty}\Bigg(Q^{l}(d_{l1},\theta_{l1},\beta_L)Q^{l}(d_{l1},\theta_{l1},\beta_R)\frac{e^{ikd_{l1}}}{d_{l1}}+Q^{l+1}(d_{l2},\theta_{l2},\beta_L)Q^{l}(d_{l2},\theta_{l2},\beta_R)\frac{e^{ikd_{l2}}}{d_{l2}}$$
$$+Q^{l}(d_{l3},\theta_{l3},\beta_L)Q^{l+1}(d_{l3},\theta_{l3},\beta_R)\frac{e^{ikd_{l3}}}{d_{l3}}+Q^{l+1}(d_{l4},\theta_{l4},\beta_L)Q^{l+1}(d_{l4},\theta_{l4},\beta_R)\frac{e^{ikd_{l4}}}{d_{l4}}$$
$$+Q^{l}(\bar{d}_{l1},\bar{\theta}_{l1},\beta_L)Q^{l}(\bar{d}_{l1},\bar{\theta}_{l1},\beta_R)Q(\bar{d}_{l1},\bar{\Theta}_{l1},\beta_G)\frac{e^{ik\bar{d}_{l1}}}{d_{l1}}+Q^{l+1}(\bar{d}_{l2},\bar{\theta}_{l2},\beta_L)Q^{l}(\bar{d}_{l2},\bar{\theta}_{l2},\beta_R)Q(\bar{d}_{l2},\bar{\Theta}_{l2},\beta_G)\frac{e^{ik\bar{d}_{l2}}}{d_{l2}}$$
$$+Q^{l}(\bar{d}_{l3},\bar{\theta}_{l3},\beta_L)Q^{l+1}(\bar{d}_{l3},\bar{\theta}_{l3},\beta_R)Q(\bar{d}_{l3},\bar{\Theta}_{l3},\beta_G)\frac{e^{ik\bar{d}_{l3}}}{d_{l3}}$$
$$+Q^{l+1}(\bar{d}_{l4},\bar{\theta}_{l4},\beta_L)Q^{l+1}(\bar{d}_{l4},\bar{\theta}_{l4},\beta_R)Q(\bar{d}_{l4},\bar{\Theta}_{l4},\beta_G)\frac{e^{ik\bar{d}_{l4}}}{d_{l4}}\Bigg), \tag{23}$$

where θ_{l1}, θ_{l2}, θ_{l3}, θ_{l4}, $\bar{\theta}_{l1}$, $\bar{\theta}_{l2}$, $\bar{\theta}_{l3}$, $\bar{\theta}_{l4}$, $\bar{\Theta}_{l1}$, $\bar{\Theta}_{l2}$, $\bar{\Theta}_{l3}$, and $\bar{\Theta}_{l4}$ are the angles of incidence of the reflected waves measured from the normal of the reflecting plane.

The validity of Eq. (23) can be confirmed by comparing it with precise model experiments conducted indoors in an anechoic chamber and outdoors in a narrow street. The details of these experimental measurements and numerical simulations will be described in the following section. Before we end this section, we remark that use of an impedance model for enclosing surfaces has somewhat complicated the analysis. However, its introduction is essential as it allows the consideration of more general situations. For instance, a hard ground is not accurate enough to model an asphalt road surface which is frequently used to reduce road traffic noise in urban areas.

III. NUMERICAL SIMULATIONS, EXPERIMENTAL RESULTS, AND DISCUSSIONS

A. Numerical simulations

To simplify the problems, we shall model the propagation of sound in city streets as an analogous situation to the determination of sound fields in a simple channel bounded by two parallel (vertical) infinite walls and a flat horizontal ground. Although it is straightforward to implement impedance boundary conditions in our numerical model, the analyses here are restricted to perfectly reflecting wall surfaces only. Both hard and impedance grounds will be studied. The width of the channel is W and the source is located at a height of z_s above the horizontal ground. To facilitate subsequent calculations, we assume that the origin coincides with the left corner of the street canyon (in the $y=0$ plane) as shown in Fig. 1. The source and receiver are located at $(x_s,0,z_s)$ and (x,y,z), respectively. We are interested in the case where $0\leqslant x,\ x_s\leqslant W$.

It is obvious from Fig. 2 that a series of image sources are produced by multiple reflections of the two parallel walls. Another set of image sources is also formed due to the presence of a reflecting ground. The total sound field can be estimated either by Eq. (13) or (23), depending on whether the incoherent or coherent models are required.

In the presentation of numerical and experimental results, we use excess attenuation (EA), which is defined as the ratio of the total field, P, to the direct field, P_d, as follows:

$$\mathrm{EA}=20\lg(P/P_d). \tag{24}$$

There are many rays connecting the source and receiver that contribute to give the total field. According to the incoherent model, the individual excess attenuation, EA_n due to each ray can be obtained from Eqs. (14) and (15) to yield

$$\mathrm{EA}_n=L_{Rn}-L_D=20\lg(d_R/d_{Rn})+10n\lg(1-\alpha), \tag{25}$$

where n is the order of rays. The excess attenuation, EA, due to the total field is obtained by combining each individual excess attenuation, EA_n logarithmically to give

$$\mathrm{EA}=10\lg\Bigg(\sum_{n=1}^{\infty}10^{\mathrm{EA}_n/10}\Bigg). \tag{26}$$

We wish to point out that only a few terms are normally required in Eq. (13), and hence Eq. (26), to ensure the convergence of the series. This is because of the large distances of the image sources from the receiver and the presence of $(1-\alpha)^n$ term in the series. Oldham and Radwan[22] suggested that the inclusion of higher orders beyond 8 (i.e., $n=8$) produced only a minor contribution to the total field, which can be ignored without significant errors. Our initial analysis supports their view. Indeed, the exact number of n depends on the distance between the source and the receiver, the separation of the boundaries, and the magnitude of the absorption coefficient. When the separation of the boundaries is reduced, it is found that up to 12th-order rays ($n=12$) are required to ensure the convergence of the series for the calculation of the total sound intensities. In Fig. 3, we display a plot of the excess attenuation, EA, versus the wall separation, W. The source and receiver are located at heights of 0.5

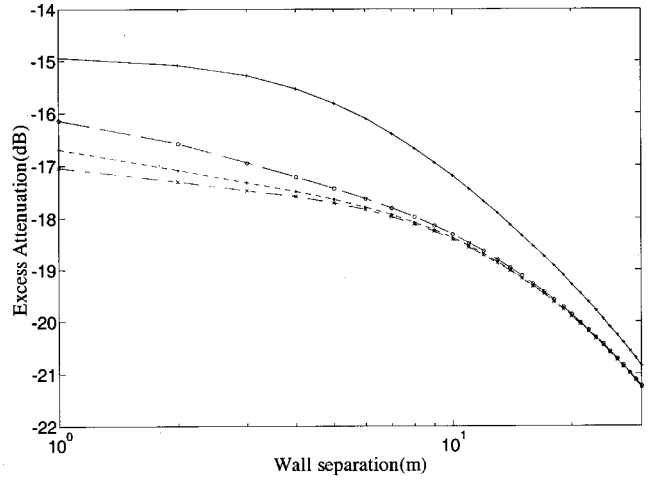

FIG. 3. The contribution of the higher-order rays on overall sound fields by plotting the predicted excess attenuation versus wall separation. The source is located at $(W/2,0,0.5)$ and receiver at $(W-1,20,1.5)$. ———, $n=4$; ---, $n=8$; ···, $n=12$; –·–, $n=16$.

and 1.5 m, respectively, above the ground, and the horizontal separation between them is 20 m. In numerical simulations, the source is placed equidistant from both vertical walls and the receiver is placed at $(W-1)$ m from the left vertical wall.

Different values of n (4, 8, 12, and 16, respectively) are used to calculate the sound intensities, which illustrate the relative significance of higher-order rays. The excess attenuation, which is defined as $L_{Rn}-L_D$ with a reference distance d_R of 1 m, is used in Fig. 3. It is obvious that there is a sizable contribution from the 8th higher-order ray and above $(n\geqslant 8)$ if W is less than about 4 m. Its contribution becomes insignificant if the separation is greater than 10 m.

Differences between noise levels with and without ground surfaces were found to be of the order of 2.5 dB within a typical urban distance of 200 m. In one of the incoherent models, further approximation is made: the ground effect is approximated by adding 3 dB to the predicted levels due to the wall reflections only.[7] Further, it is interesting to note that the excess attenuation, the total field in the incoherent model, is independent of the frequencies since the absorption coefficients of all reflecting surfaces are assumed to be constant at all frequencies. We reiterate here that the absorption coefficient of 0.1 is taken in our numerical simulations.

According to the coherent model, the total field, P, can be obtained from Eq. (23). It is worth noting that the spherical wave reflection coefficient is equal to 1 for a perfectly reflecting surface. In this case, Eq. (23) can be reduced to Eq. (11). No further simplification can be made if the total sound field is computed by summing all contributions from individual rays coherently. It is straightforward to use Eq. (23) to compute the sound pressure. Hence the excess attenuation can be determined by using Eq. (24) with the direct field given by

$$P_d=\frac{1}{4\pi}\left[\frac{e^{ikd_R}}{d_R}\right], \tag{27}$$

where d_R is the direct distance between the source and receiver. In laboratory measurements and theoretical predictions, d_R is taken to be 1 m for the reference sound level.

A close examination of Eq. (23) reveals that the sound field is calculated by summing an infinite series. Each term of the series is represented by a ''virtual'' source multiplied by a spherical wave reflection coefficient. As discussed previously, only a finite number of image sources contribute significantly to the total sound field. The contributions of these image sources, which become weaker in strength when they are located farther from the receiver, can be neglected. The rate of attenuation is even greater for boundaries of finite impedance since the spherical wave reflection coefficient is generally less than 1 for such cases. Hence, the strength of the reflected waves is further attenuated after a few reflections from the boundaries. In our experiments, as shown in the following sections, we find that the use of 8 to 12 sets of image sources in our theoretical predictions is normally adequate to give satisfactory results.

Figure 4 shows a comparison of the theoretical predictions for sound propagation in street canyons. The predicted excess attenuation is plotted against the width of the street canyon. The source frequencies of 125 Hz, 1 kHz, and 8 kHz are used in the coherent model for the prediction of sound fields. In Fig. 4(a), the source and receiver coordinates are set at $(W/2,0,0.65)$ and $(W/2,5,2.4)$, respectively. A somewhat different receiver location of $(W-1,10,5)$ is used in Fig. 4(b). Figures 4(a) and (b) show that coherent and incoherent models give rather similar results when the width of a street canyon is greater than about 10 m. However, when the width becomes narrower, deviations in EA as predicted by the coherent and incoherent models are more significant. This suggests that it is inappropriate to use the incoherent model for the prediction of noise propagation in a narrow street canyon.

B. Indoor laboratory measurements

In the present study, a one-tenth scale was used to model a street canyon and a data acquisition system was set up to conduct indoor measurements for sound propagation over different ground surfaces. A BSWA TECH $\frac{1}{2}$-in. condenser prepolarized microphone of type MK224 fitted with a BSWA TECH preamplifier of type MA201 was used as the receiver for indoor measurements. A Tannoy driver with a tube of internal diameter of 3 cm and length of 1.5 m was used as a point source. All indoor measurements were conducted in an anechoic chamber with internal dimensions of $6\times6\times4$ m^3. A PC-based maximum length sequence system analyzer (MLSSA)[23] was used both as the signal generator for the source and as the analyzer for subsequent data processing. The received signals were compared with the known output sequence such that the background noise effects were minimized. The time-domain data were converted to spectrum level data through the use of fast Fourier transform. Each spectrum level was then normalized by a ''standard'' prerecorded direct field measurement. All the steps described above were carried out with MLSSA software. The final output was the required excess attenuation spectrum. We note

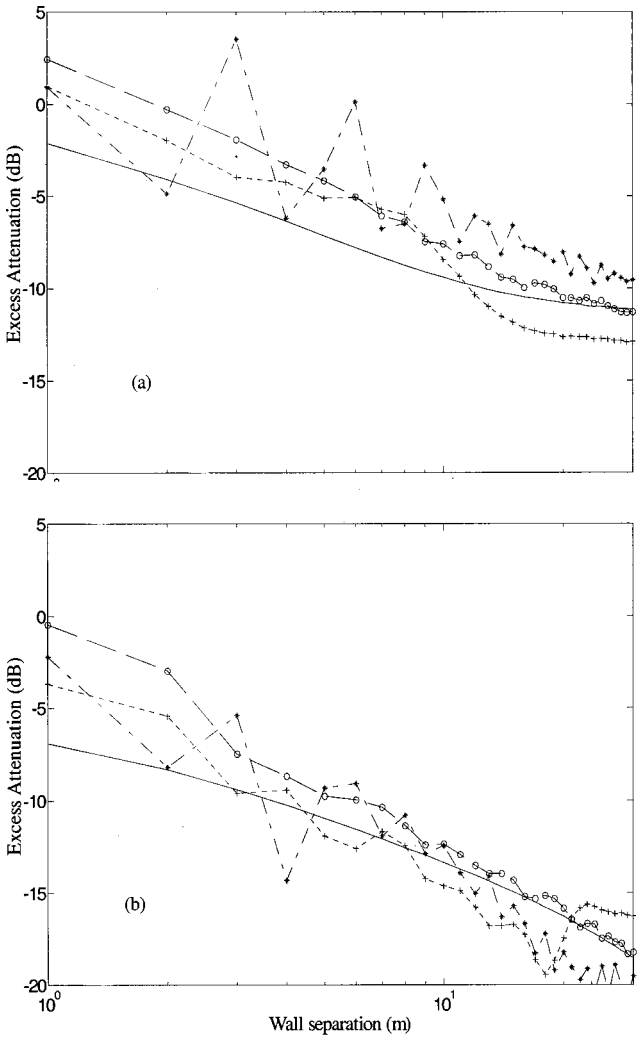

FIG. 4. Comparisons of the coherent and incoherent prediction on the excess attenuation versus wall separation. *−−−*, coherent prediction at 125 Hz; +----+, coherent prediction at 1000 Hz; ∘−−∘, coherent prediction at 8000 Hz; ———, incoherent prediction. (a) Both source and receiver are located at the centerline. The coordinates of the source and receiver are $(W/2,0,0.65)$ and $(W/2,5,2.4)$. (b) The source is located at the centerline and the receiver is offset from the centerline. The coordinates of the source and receiver are, respectively, $(W/2,0,0.65)$ and $(W-1,10,5)$.

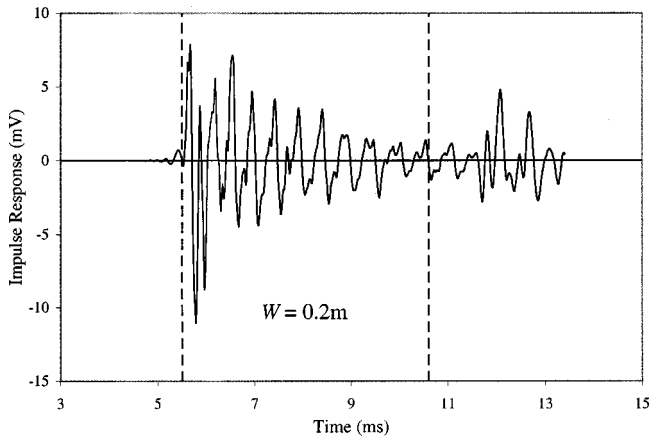

FIG. 5. The impulse response at the receiver for the direct ray up to the 12th-order ray; source at (0.1,0,0.065) and receiver at (0.1,0.8,0.065).

that the prerecorded direct field measurement is taken at 1 m from the source in the absence of any reflecting surfaces in the anechoic chamber.

In the current study, the maximum length sequence (MLS) technique is chosen to investigate sound propagation in a model street canyon as the technique improves the signal-to-noise ratio as compared to the conventional, stationary excitation technique. Heutchi *et al.*[24] have confirmed its usefulness in their study of outdoor sound propagation for distances of up to 200 m.

MLSSA operates in the time domain where the impulse response is measured. As we are only interested in reflection rays up to 12th order, the time-domain data chosen for processing are based on the time between the arrival of the direct and the 12th-order rays. Figure 5 shows a typical impulse response for sound propagation in a model street canyon for the source and receiver located at (0.1,0,0.065) and (0.1,0.8,0.065), respectively. For this particular source/receiver geometry, a time interval of between 5.5 and 10.6 ms is chosen for our subsequent analysis in the frequency domain, as the former is estimated to be the arrival time of the direct ray, while the latter is that for the 12th-order ray.

A varnished plywood board 18 mm in thickness was used to simulate an acoustically hard surface. A carpet, laid on the varnished plywood board, was used to simulate an impedance ground surface. Preliminary measurements were conducted for sound propagation over the plywood board. Both source and receiver were set at a height of 0.065 m above the surface at various receiver locations between 0.5 and 1.4 m from the source. Theoretical predictions of excess attenuation based on the model described in the previous section were in accord with the experimental results. A typical set of measurements, with a source/receiver separation of 0.5 m, is shown in Fig. 6(a).

Attenborough's two-parameter model[25] was used to describe the impedance of the ground surface. Measurement procedures were repeated as in the case of the hard surface described above. The two parameters, the effective flow resistivity (σ_e) and the effective rate of change of porosity with depth (α_e), were deduced from the measurements. The best-fit values for σ_e and α_e were 13.5 kPa s m^{-2} and 100 m^{-1}, respectively. Figure 6(b) shows a comparison of experimental results and theoretical predictions based on the best-fit parameters for the acoustical characterization of the absorbing ground—a carpet laid on a plywood board. We note that, in Fig. 6(b), the same source/receiver geometry was used as in Fig. 6(a).

After the acoustical characterization of the model ground, a one-tenth scale model of a street canyon was set up in the anechoic chamber. Since the maximum path length between the image source and the receiver was about 10 m (100 m at full scale) at frequency up to 10 kHz in our measurements, the effect of air absorption was not included in our analyses. The vertical walls and ground were made of 18-mm-thick plywood boards. The vertical walls, which were supported by a steel angle framework to ensure their orientation and stability, have a length and height of 2.4 and 1.8 m, respectively. The separation, W, between the vertical walls was set at 0.2, 0.5, and 0.8 m for experiments. In a set

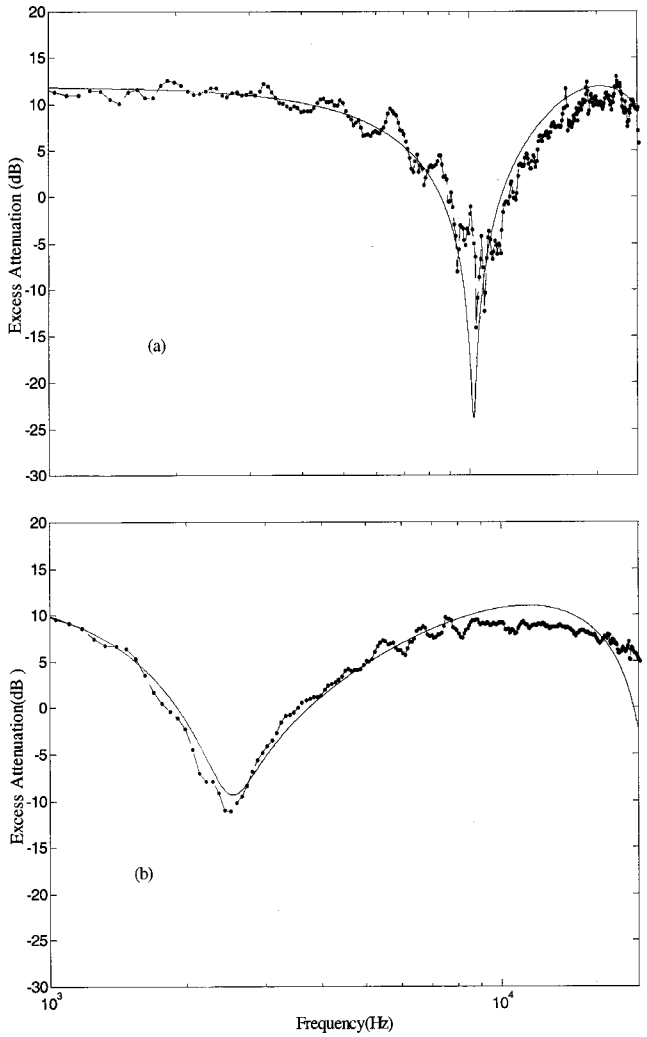

FIG. 6. Sound propagation over horizontal ground. Both source and receiver are 0.065 m above the ground and are separated from each other at 0.5 m. ——— theoretical prediction; ---, measurement. (a) Effect of hard ground reflection and (b) characterization of impedance ground.

of measurements, carpet was laid on the plywood board to simulate an absorbing ground surface in a street canyon.

At full scale, the model represents a canyon street section of 24 m in length with two 18-m-high flat vertical parallel building walls erected on either side of a street with widths of 2, 5, and 8 m. In the following paragraphs, we refer to all dimensions as the scaled distances unless otherwise stated. Although Busch *et al.*[26] have reported an improved technique for simultaneously selecting both an optimal scale factor and optimal model materials, no attempt is made in our laboratory measurements to select the most appropriate materials to model an outdoor porous ground surface. However, the use of carpet-covered ground will allow a validation of the coherent and incoherent models by comparing theoretical predictions with precise indoor measurements.

Indoor measurement of the excess attenuation was made at various receiver locations with the source located near the ground. This is to simulate the approximate location of ground-based sources such as engine noise emitted from light vehicles or other construction equipment for road repair

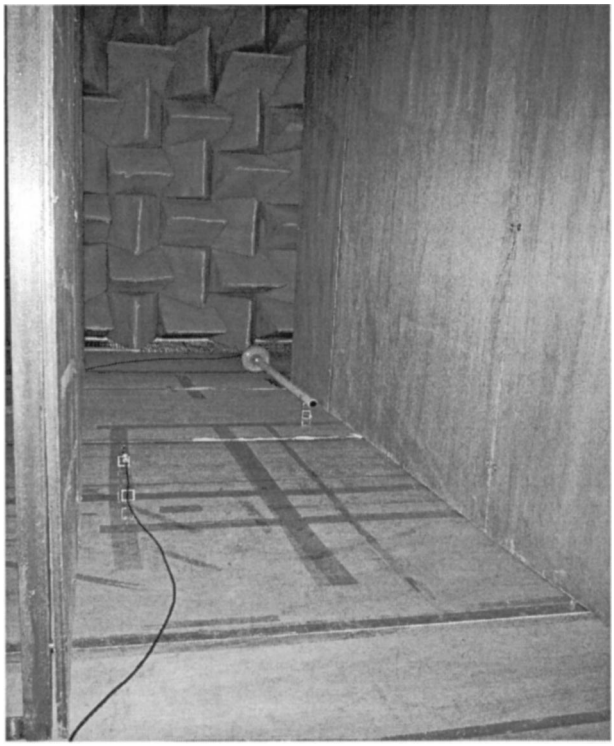

FIG. 7. A 1:10 scale model set up in an anechoic chamber for measurement of sound propagation in a street canyon.

work. Recently, Horoshenkov *et al.*[27] have used a 1:20 scale model to study sound propagation in a city street canyon. Noise sources, such as light and heavy vehicles, have been simulated by tubes from the source chambers elevated at 0.025 m (0.5 m at full scale) and 0.05 m (1.0 m at full scale) above the ground. In our measurements, the source was located at 0.065 m (0.65 m at full scale) above the ground and either at the centerline or on the side of the street at 0.1 m (1.0 m at full scale) from one of the vertical walls. Again, the chosen source height was used to simulate a realistic urban noise source such as the typical engine location of automobiles. For the 0.2-m-wide street, the receivers were set to locate both at the centerline of the street and on the side of the street at 0.02 m from one of the vertical walls. For the 0.5- and 0.8-m-wide streets, the receivers were also set at the centerline and on the side of the street but at 0.1 m from one of the vertical walls. The heights of the receivers were at 0.065, 0.12, 0.24 and 0.5 m from the ground. Due to the limitation of the available space in the anechoic chamber, the horizontal distances between the source and receivers were in the range of 0.2 to 1.0 m. A photograph showing the scale model set in the anechoic chamber is shown in Fig. 7.

To demonstrate the effect of mutual interference, the source was placed equidistant from the vertical walls and at a height of 0.065 m. Measurements were taken at a horizontal distance of 1 m in front of the source and at a height of 0.5 m above the ground. By reducing the width of the street, the interference effect became more significant. Figure 8(a) shows that distinct peaks occurred at 2000 and 6000 Hz (200 and 600 Hz at full scale) in the street of width 0.2 m (2 m at full scale). In this event, the measured excess attenuation caused by constructive interference is 10 dB higher than that

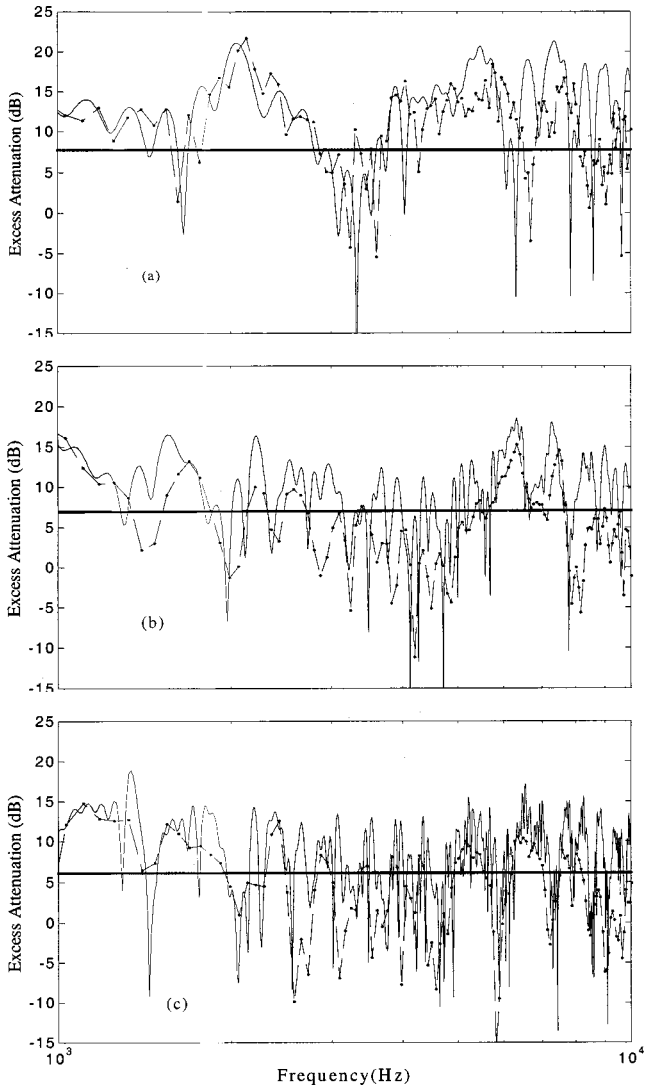

FIG. 8. Excess attenuation versus frequency for various street widths for hard ground. ———, coherent prediction; ———, incoherent prediction; ·——·, measurement. (a) Width=0.2 m; source at (0.1,0,0.065); receiver at (0.1,1,0.5); (b) width=0.5 m; source at (0.25,0,0.065); receiver at (0.25,1,0.5); and (c) width=0.8 m; source at (0.4,0,0.065); receiver at (0.4,1,0.5).

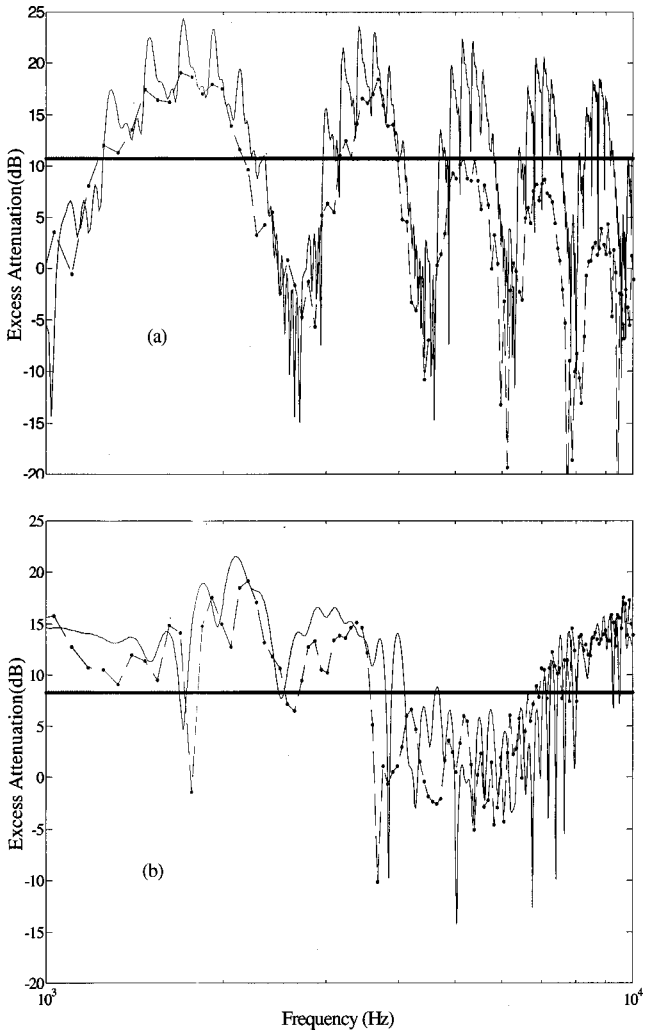

FIG. 9. Excess attenuation versus frequency for different ratios of the horizontal distance to street width. A hard ground is assumed in the prediction. ———, coherent prediction; ———, incoherent prediction; ·——·, measurement. (a) Ratio=0.25; width=0.8 m; source at (0.1,0,0.065); receiver at (0.7,0.2,0.065); and (b) ratio=5; width=0.2 m; source at (0.1,0,0.065); receiver at (0.18,1,0.24).

predicted by the incoherent model. In Figs. 8(b) and (c), peaks and dips are close to each other and such fluctuations will be smoothed out if the measurements are taken in octave bands. This shows that the interference effect becomes gradually less significant when the width of the street is increased to 0.5 and 0.8 m (5 and 8 m for a full-scale street).

The interference effect can also occur when the source is located at positions other than the center. In Fig. 9, the source is located 0.1 m from one of the vertical walls and the receiver is placed at 0.1 or 0.02 m from the opposite wall. To further demonstrate that the coherent model can be used to predict the interference effect in a wide range of horizontal distances to street width ratios, a change in the ratio from 0.25 to 5.0 is selected for the purpose of illustration. The theoretical and experimental results are shown in Figs. 9(a) and (b), respectively. In Fig. 9(a), the horizontal distance between the source and receiver is set at 0.2 m (the shortest distance used in the experiment) in the 0.8-m-wide street (the widest street used in the experiment). In Fig. 9(b), the horizontal distance is 1.0 m (the longest distance used in the experiment) in the 0.2-m-wide street (the narrowest street used in the experiment).

Elevated noise sources, such as air conditioners and cooling towers, installed on building facades are common in a complex urban environment. To simulate this situation, additional measurements of the excess attenuation were made for the street canyon with width of 0.5 m. The source was located at 0.05 m (0.5 m at full scale) from one of the vertical walls and the receivers were placed at 0.1 m from the opposite wall. While the source was set at 0.5 m (5 m at full scale) above the ground, the receivers were set at the heights of 0.15, 0.5 and 0.8 m. The horizontal distances between the source and receivers were set at 0.2, 0.5, 0.8 and 1 m.

The effect of mutual interference also occurs when the noise is emitted from the elevated source. Figure 10(b) illustrates that a distinct dip occurs at around 1700 Hz (170 Hz at full scale) when the receiver is located at the same height of the source. When the receiver is moved to either a lower

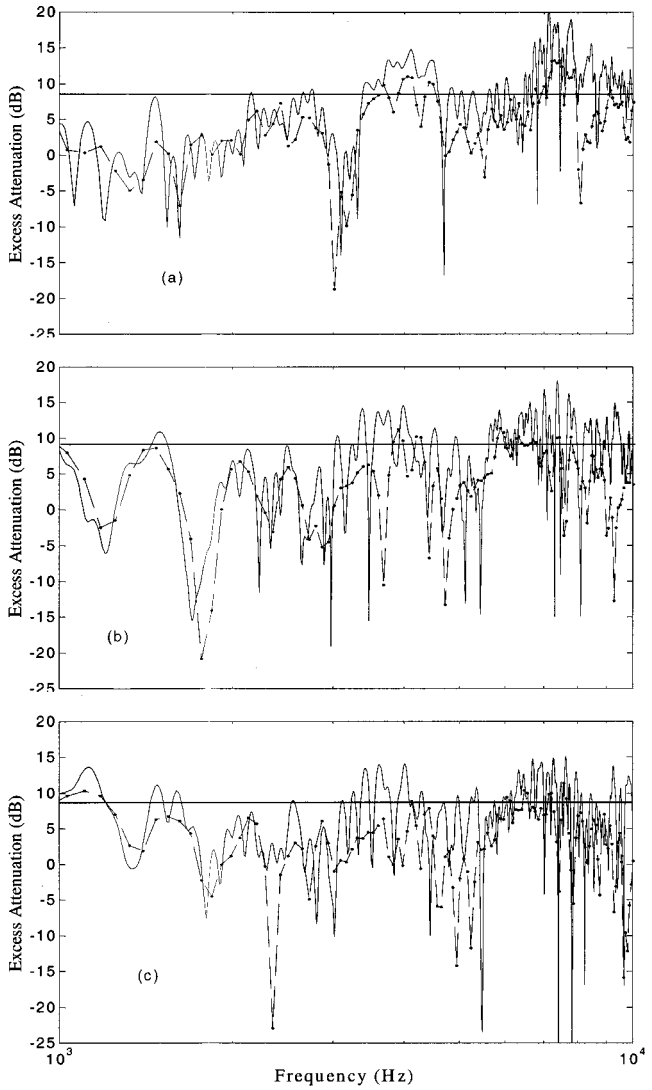

FIG. 10. Excess attenuation versus frequency for elevated source in a 0.5-m-wide street with hard ground. ———, coherent prediction; ——, incoherent prediction; ·——·, measurement. (a) Source at (0.05,0,0.5); receiver at (0.4,0.8,0.15); (b) source at (0.05,0,0.5); receiver at (0.4,0.8,0.5); and (c) source at (0.05,0,0.5); receiver at (0.4,0.8,0.8).

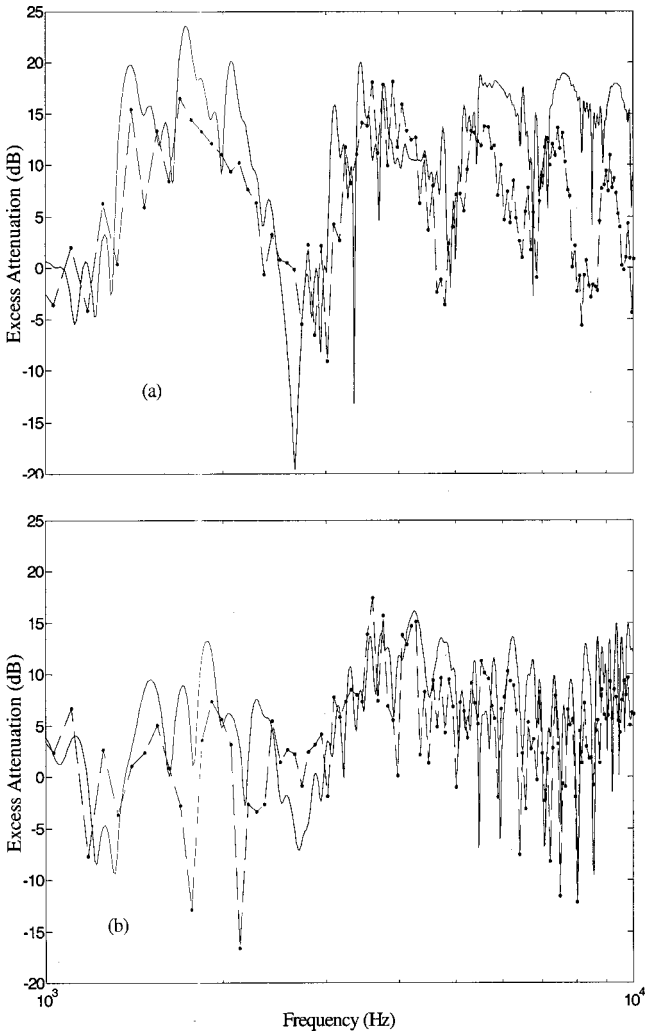

FIG. 11. Excess attenuation versus frequency for various receiver locations in the street with an impedance ground. ———, coherent prediction; ·——·, measurement. (a) Width=0.5 m; source at (0.1,0,0.065); receiver at (0.4,0.2,0.12); and (b) width=0.5 m; source at (0.1,0,0.065); receiver at (0.4,1,0.5).

level at 0.15 m above the ground in the scale model experiment in Fig. 10(a) or to a higher level at 0.8 m above the ground in Fig. 10(c), the effect of destructive interference becomes less significant. In Figs. 10(a)–(c), the source is separated from the receiver at a horizontal distance of 0.8 m. According to the incoherent model the predicted results will be the same in all the cases. However, it is worth pointing out that there are about 10 dB differences between the prediction results by the incoherent model and the measurements at the frequency range from 1000 to 2000 Hz (100 to 200 Hz at full scale).

The coherent model can also be used to predict the interference peaks and dips in the street with an absorptive ground. Experiments were conducted in the ''model'' street at the anechoic chamber. To compare the numerical and experimental results, the predicted excess attenuation together with the measured excess attenuation are plotted against the frequency in Figs. 11(a) and (b). In these comparisons, the width of the street was 0.5 m and the source was located 0.1 m from one of the vertical walls while the receiver was located 0.1 m from the opposite wall. Furthermore, the receiver was set at a horizontal distance of 0.2 m from the source and at 0.12 m above the ground in Fig. 11(a), and was moved to 1.0 m from the source and 0.5 m above the ground in Fig. 11(b). Again, good agreements between the theoretical predictions and experimental measurements are evident from the results as shown in the figures. The agreements are within 5 dB in most cases, especially at the frequency range from 3000 to 5000 Hz (300 to 500 Hz at full scale). However, the most important point to note is that the numerical model can predict well the general trend of the experimental data in the frequency spectrum.

Although it is increasingly common to use porous asphalt[28] as a noise abatement measure for reducing traffic noise, it may not be useful in some frequency ranges. Figure 12 illustrates that the sound levels are increased significantly at the frequency range of 3000 to 4000 Hz by the introduction of a finite impedance ground. Figure 12(a) shows the excess attenuation when measurements are conducted in a street of width 0.5 m with a plywood board representing hard

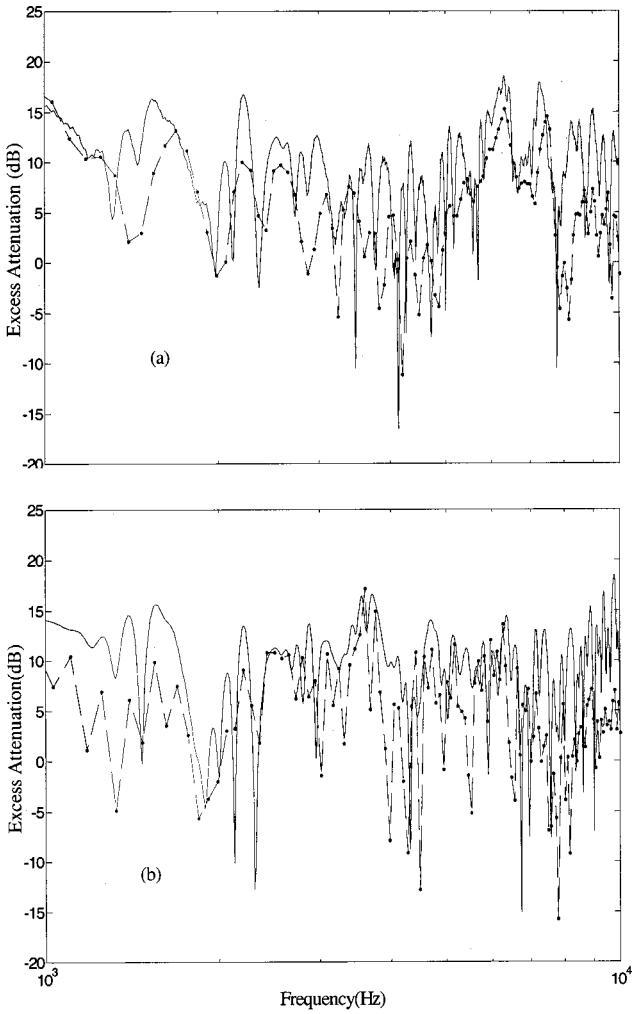

FIG. 12. Comparison of excess attenuation with the boundary conditions changing from (a) a hard ground to (b) an impedance ground. ———, coherent prediction; ·––·, measurement. In both cases, the width=0.5 m, the source is at (0.25,0,0.065), and receiver at (0.25,1,0.5).

ground. Figure 12(b) displays the results obtained in the same street with a carpet-covered board representing an absorbing ground. In both cases, the source and the receiver are placed equidistant from the vertical walls. The source is set at a height of 0.065 m. The receiver is located at a height of 0.5 m and at a horizontal distance of 1.0 m from the source.

In general, the theoretical predictions by the coherent model agree reasonably well with the indoor experimental data, which suggests that the interference effect should not be ignored, especially for narrow street canyons. Some discrepancies are found at frequencies between 1000 and 2000 Hz in the scale model experiments. This is probably due to the experimental limitations in the anechoic chamber and the diffraction effect at the edges of the scale model. We also note that some systematic discrepancies are observed in the high frequency region above 10 000 Hz (1000 Hz at full scale). In this region, experimental results are always lower than the predictions.

We also wish to point out that some indoor experimental results are presented in single frequencies for different wall separations. This allows clear and detailed comparisons of experimental data with the numerical models in a more precise manner. However, in the next section, we shall show outdoor data where experimental results will be presented in one-third octaves from the practical point of views.

FIG. 13. Experimental setup in a 1.55-m-wide street canyon for outdoor measurements.

C. Outdoor field measurements

We have demonstrated in the last section that the coherent model agrees well with indoor measurement data. To provide further evidence in a realistic urban environment, outdoor experimental measurements are required in order to establish the validity of the coherent model for the prediction of multi-path transmissions of sound in a street canyon. A side lane of 1.55 m in width was chosen. Two parallel building facades furnished with marble stone and ceramic tiles enclosed the side lane. The ground was made of concrete with a small drain channel formed at the edge of the side lane (see Fig. 13 for a photograph of the experimental test site).

A Roland type KC-300 amplifier and loudspeaker unit was used as the sound source. A broadband white noise, which was generated by an Ivie Noise Generator of type IE-20B, was used for all outdoor experiments. Measurements of the sound pressure levels in one-third octave bands were conducted using an Ono Sokki Precision Sound Level Meter type LA-5110 at various receiver locations, with the source situated at the centerline of the side lane and 0.5 m above the ground. The receiver was located either at the centerline of the street or at an offset position of 0.15 m from one of the building facades.

It is convenient to present the outdoor experimental data in a form of ''transmission loss'' spectrum for comparison with the theoretical predictions. The transmission loss (TL) is defined as the ratio of the total sound field, P is measured at the receiver position to the total sound field, and P_1 is measured at 1 m from the source at the same height. It can be expressed as

$$\mathrm{TL}=20\lg(P/P_1). \tag{28}$$

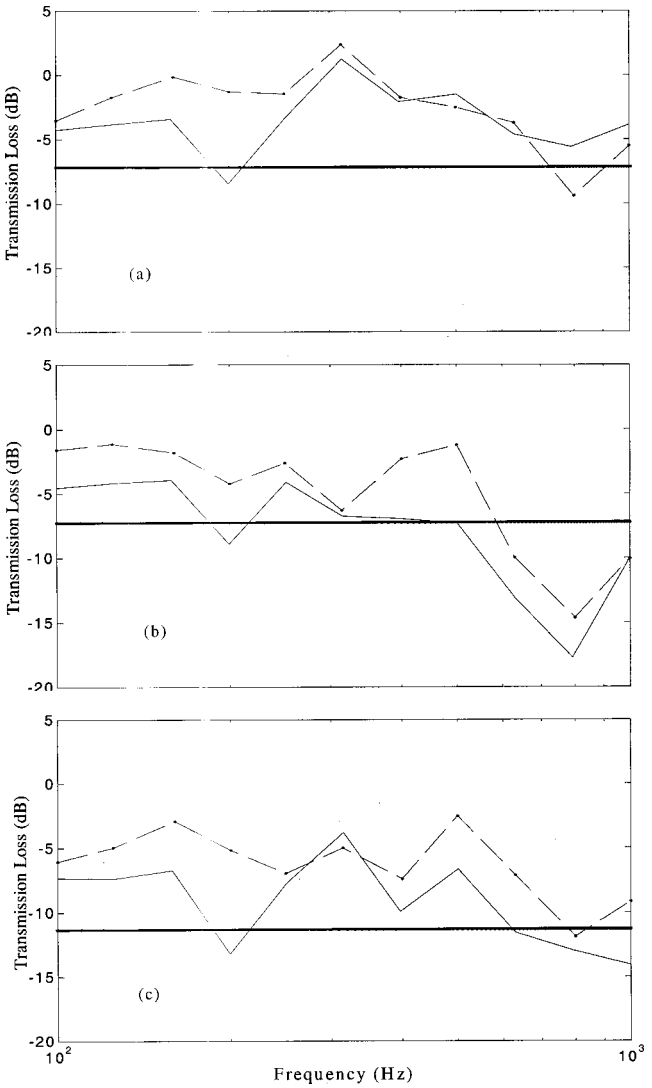

FIG. 14. Comparison of transmission loss spectra among the coherent model predictions, the incoherent model predictions, and outdoor measurements for a street canyon with a width of 1.55 m. ———, coherent prediction; ———, incoherent prediction; ·––·, measurement. (a) Source at (0.78,0,0.5); receiver at (0.78,3.88,0.5); (b) source at (0.78,0,0.5); receiver at (1.4,3.88,0.93); and (c) source at (0.78,0,0.5); receiver at (0.78,7.75,1.86).

Figure 14 (see the figure captions for the geometrical configurations of the source and receiver) shows comparisons of the theoretical predictions with the outdoor experimental results. We note that the theoretical predictions of sound propagation in the side lane in one-third octave bands are based on the coherent model as well as the incoherent model. Due to the limitation of the test site in our outdoor measurements, the horizontal distances between the source and the receiver are limited in the range from 1.0 to 7.75 m and all boundaries are modeled as perfectly reflecting planes. Nevertheless, the experimental results can provide us with useful information on the validity of the model in a more complex outdoor environment.

It is found from Figs. 14(a)–(c) that the coherent model can give a reasonable prediction of the general trend of the transmission loss spectra as compared with the experimental data. However, the incoherent model is unable to predict the trend because the interference effects from all contributing rays are ignored in this model. Inevitably, the incoherent model will not be sufficiently accurate when it is used to predict the propagation of sound in a narrow street canyon. In fact, we have conducted a series of measurements for other geometrical configurations as described earlier. In this paper, we only show three sets of representative data for illustration. All other measurements have led to a rather similar conclusion as described above. Hence, they are not shown here for the sake of brevity.

Finally, some significant discrepancies between outdoor measurements and theoretical predictions are found. In addition to the possible reasons explained in the last section, there are some possible factors that might affect the accuracy of outdoor measurements as follows,

(1) The surface roughness of the building facades and the drain channels on the ground could cause diffusion of sound;
(2) sound might reflect back from both ends of the side lane; and
(3) the atmospheric turbulence effect is especially important at high frequencies above 4000 Hz octave band. As a result, the predicted attenuation will be less reliable especially at high frequencies.

IV. CONCLUSIONS

Theoretical models of the sound field due to a stationary, point monopole source in a street canyon have been developed. The theory is an extension of the classical Weyl–van de Pol formula that includes the effect of multiple reflections from boundary surfaces. By identifying the corresponding image sources, the total field can be computed by summing all contributions coherently. Indoor experiments have been conducted in a one-tenth scale model facility. Locations of the source and the receiver are chosen to simulate those situations commonly occurring in city streets. It has been demonstrated that the theoretical predictions agree reasonably well with our experimental measurements. Further, outdoor experimental measurements have also been conducted to establish the validity of the proposed model for the prediction of multi-path transmissions of sound in a street canyon.

It is concluded that the interference effect has to be taken into account to predict the sound propagation in narrow street canyons of perfectly flat walls. Use of the incoherent model gives reasonable predictions only when the separation between the two vertical walls of a street canyon is greater than 10 m or in the case when there are structured walls leading to significant diffusions of sound energy.

ACKNOWLEDGMENTS

One of the authors (KKI) is supported by a Teaching Company Scheme jointly sponsored by the Industry Department of the HKSAR Government and NAP Acoustics (Far East) Limited. The research described in this paper was supported in part by the Hong Kong Polytechnic University and the Research Grants Council of the HKSAR Government.

[1] J. E. Piercy, T. F. W. Embleton, and L. C. Sutherland, ''Review of noise propagation in the atmosphere,'' J. Acoust. Soc. Am. **61**, 1403–1418 (1977).
[2] T. F. W. Embleton, ''Tutorial on sound propagation outdoors,'' J. Acoust. Soc. Am. **100**, 31–48 (1996).
[3] W. R. Schlatter, ''Sound power measurement in a semi-confined space,'' M.S. thesis, MIT, 1971.
[4] K. P. Lee and H. G. Davies, ''Monogram for estimating noise Propagation in urban areas,'' J. Acoust. Soc. Am. **57**, 1477–1480 (1975).
[5] R. H. Lyon, ''Stochastics and environmental noise,'' The 3rd US–Japan Joint Seminar in Applied Stochastics (1971).
[6] P. Steenackers, H. Myncke, and A. Cops, ''Reverberation in town streets,'' Acustica **40**, 115–119 (1978).
[7] D. J. Oldham and M. M. Radwan, ''Sound propagation in city streets,'' J. Build. Acoust., **1**, 65–88 (1994).
[8] J. Kang, ''Sound propagation in street canyons: Comparison between diffusely and geometrically reflecting boundaries,'' J. Acoust. Soc. Am. **107**, 1394–1404 (2000).
[9] RAYNOISE User's Manual, Version 2.1 LMS Numerical Technologies (2001).
[10] E. Walerian, R. Janczur, and M. Czechowicz, ''Sound level forecasting for city-centers. Part 1: Sound level due to a road within an urban canyon,'' Appl. Acoust. **62**, 359–380 (2001).
[11] M. Gensane and F. Santon, ''Prediction of sound fields in rooms of arbitrary shape: the validity of the image sources method,'' J. Sound Vib. **63**, 97–108 (1979).
[12] G. Lemire and J. Nicolas, ''Aerial propagation of spherical sound waves in bounded spaces,'' J. Acoust. Soc. Am. **86**, 1845–1853 (1989).
[13] S. M. Dance, J. P. Roberts, and B. M. Shield, ''Computer prediction of sound distribution in enclosed spaces using an interference pressure model,'' Appl. Acoust. **44**, 53–65 (1995).
[14] S. H. Tang and K. M. Li, ''The prediction of facade effects from a point source above an impedance ground,'' J. Acoust. Soc. Am. **110**, 278–288 (2001).
[15] J. Lighthill, ''Asymptotic behaviour of anisotropic wave systems stimulated by oscillated sources,'' in *Wave Asymptotics*, edited by P. A. Martin and G. R. Wickham (Cambridge U. P., Cambridge, 1992), Chap. 1. See also J. Lighthill, ''Emendations to a proof in the general three-dimensional theory of oscillating sources of waves,'' Proc. R. Soc. London, Ser. A **427**, 31–42 (1990).
[16] L. M. Brekhovskikh, *Waves in Layered Media* (Academic, New York, 1980), p. 228.
[17] S. O. Benjegard, ''Traffic noise in urban areas,'' The 8th International Congress on Acoustics, London (1974), p. 114.
[18] C. H. Chew, ''Prediction of traffic noise from expressways—Part II: Buildings flanking both sides of expressway,'' Appl. Acoust. **32**, 61–72 (1991).
[19] H. G. Davies, ''Multiple-reflection diffuse-scattering model for noise propagation in streets,'' J. Acoust. Soc. Am. **64**, 517–521 (1978).
[20] M. E. Delany, ''Prediction of traffic noise levels,'' NPL Acoustic Report 56 (1972).
[21] K. Attenborough, ''Review of ground effects on outdoor sound propagation from continuous broadband sources,'' Appl. Acoust. **24**, 289–319 (1988).
[22] M. M. Radwan and D. J. Oldham, ''The prediction of noise from urban traffic under interrupted flow conditions,'' Appl. Acoust. **21**, 163–185 (1987).
[23] D. D. Rife and J. Van der Kooy, ''Transfer-function measurement with Maximum-Length Sequences,'' J. Audio Eng. Soc. **37**, 419–443 (1989).
[24] K. Heutschi and A. Rosenheck, ''Outdoor sound propagation measurements using an MLS Technique,'' Appl. Acoust. **51**, 13–32 (1997).
[25] K. Attenborough, ''Ground parameter information for propagation modelling,'' J. Acoust. Soc. Am. **92**, 418–427 (1992).
[26] T. A. Busch and M. R. Hodgson, ''Improved method for selecting scale factors and model materials for scale modelling of outdoor sound propagation,'' J. Sound Vib. **243**(1), 173–181 (2001).
[27] K. V. Horoshenkov, D. C. Hothersall, and S. E. Mercy, ''Scale modelling of sound propagation in a city street canyon,'' J. Sound Vib. **223**(1), 795–819 (1999).
[28] M. C. Berengier, M. R. Stinson, G. A. Daigle, and J. F. Hamet, ''Porous road pavements: Acoustical characterization and propagation effects,'' J. Acoust. Soc. Am. **101**, 155–162 (1997).